Grande, Rafael; Bai, Long; Wang, Ling; Xiang, Wenchao; Ikkala, Olli; Carvalho, Antonio J.F.; Rojas, Orlando J.

Nanochitins of Varying Aspect Ratio and Properties of Microfibers Produced by Interfacial Complexation with Seaweed Alginate

Published in:
ACS Sustainable Chemistry and Engineering

DOI:
10.1021/acssuschemeng.9b06099

Published: 21/01/2020

Document Version
Peer-reviewed accepted author manuscript, also known as Final accepted manuscript or Post-print

Nanochitins of varying aspect ratio and properties of microfibers produced by interfacial complexation with seaweed alginate

Rafael Grande[1,2], Long Bai[2], Ling Wang[2], Wenchao Xiang[2], Olli Ikkala[2,3], Antonio J. F. Carvalho[1], Orlando J. Rojas[2,3,4,]*

(1) Department of Materials Engineering, São Carlos School of Engineering, University of São Paulo, Av. João Dagnone, 1100, 13563-120, São Carlos - SP – Brazil.

(2) Department of Bioproducts and Biosystems, School of Chemical Engineering, Aalto University, P.O. Box 16300, FIN-00076 Aalto, Espoo, Finland

(3) Department of Applied Physics, School of Science, Aalto University, P.O. Box 16300, FIN-02150 Espoo, Finland

(4) Departments of Chemical & Biological Engineering, Chemistry and, Wood Science, 2360 East Mall, The University of British Columbia, Vancouver, BC V6T 1Z3, Canada.

KEYWORDS: chitin nanofibers; sodium alginate; interfacial complexation; fiber spinning; nanoparticle aspect ratio; dry spinning

ABSTRACT

Here we introduce chitin nanofibers, nanochitin (ChNF), whose cationic groups electrostatically complex in aqueous media with the anionic groups of a polyanion, seaweed alginate (SA). This allows the formation of continuous microfibers after drawing contacting suspensions. We elucidate the effect of the nanofiber aspect ratio (15, 25 and > 60) on the mechanical performance of the composite microfibers after considering variables such as concentration, pH and drawing rate. An automatic collector facilitated a constant spinning velocity of 30 mm/s upon interfacial complexation from aqueous media (using 0.3 to 1 wt% as mass fraction for each component and a pH between 4 and 7). The composite microfibers showed a core-shell structure where ChNFs were preferentially axially aligned in the center and more randomly oriented in the shell. The degree of ChNF alignment in the core increased with the aspect ratio, as resolved by WAXS diffractograms. Consequently, ChNF with the largest aspect ratio (> 60) was readily spun into microfibers that displayed the highest Young's modulus (4.5 GPa), almost double than that measured for the shortest ChNF. The latter, however, presented the highest strain and flexibility and allowed continuous fiber spinning. Distinctively, tensile tests revealed mechanically stable microfibers even in wet condition, with a strength loss of less than 50% and strain gains of up to 35%. The amino and carboxyl groups in the microfibers offer possibilities for functionalization, expanding their potential beyond that related to wound healing and antibacterial applications. Overall, we provide a new perspective toward dry spinning *via* interfacial complexation of biobased components and the effect of particle's morphology on the detailed structuring of microfibers, which display a particular assembly that is discussed here for the first time.

INTRODUCTION

Fibers from renewable sources are essential in the development of new generation functional materials. Wound dressing, drug delivery, and tissue engineering are among the prospective applications relevant to such fibers, for instance, those based on chitin, chitosan, or nanochitin, taken their wound-healing and antimicrobial functionalities.[1–4] Chitin and alginate are highly abundant renewable materials with interesting properties. Sodium alginate, an anionic polysaccharide, is an attractive material for functional compounds in biomedical and pharmaceutical fields due its particular physicochemical properties and biological activities. Also, chitin has been widely investigated as a potential biomaterial for biomedical and bioengineering purposes due its low toxicity and antimicrobial functionality. Chitin is bio-absorbable and bears amino groups that are otherwise absent in most non-protein systems. Combining the properties of alginate with the antimicrobial and mechanical performance of nanochitin could result in a promising functional composite fiber for development of structural biomaterials. Wound dressing, drug delivery, and tissue engineering are among their prospective applications. Several approaches are available for the fiber synthesis, including electrospinning, wet- and dry-spinning, bio-spinning, microfluidic spinning, and melt-spinning (extrusion). Among these, dry-spinning, which exploits ionic interactions between polymers bearing opposite charges remains as a promising route. In this direction, the concept of polyion complexation between oppositely charged chitosan and gellan were introduced in 1998 and allowed several structural materials, including filaments.[5] The process, more commonly referred to as "interfacial polyelectrolyte complexation" (IPC), exploited the spontaneous self-assembly of the polymers into fibers by simply drawing the complex formed at the fluid-fluid interface.[6,7] The drawing process was conducted using aqueous systems under room conditions where no coagulation or anti-solvents were needed, offering

several processing advantages over the traditional spinning methods. It was also demonstrated that IPC fibers could be obtained combining nanosheets and polyelectrolytes.[8] Recently, the interest in dry-spinning of fibers was expanded into the complexation of a macromolecular solutions (for example, chitosan in water) with a nanocellulose colloidal dispersion, leading to relatively strong composite microfibers.[9,10] Subsequently, the process is referred to as "interfacial polyelectrolyte-nanofiber complexation" (IPNC). The case of spun fibers based on oppositely charged nanofibers has also been reported.[11] Overall, filaments obtained through the complexation of nanofibers has emerged as an extension to IPC systems, providing a broader perspective for their use. The process, however, is still in its infancy and has encountered several challenges, for example to develop a scalable and continuous spinning process with acceptable properties. Moreover, little is known about the effects of the components, including nanofiber morphology, on the properties of the IPNC filaments or composite microfibers. Relevant to this effort is the impact of the nanofiber aspect ratio on the spinnability and mechanical properties of the IPNC.

In this work, an IPNC system comprising cationic chitin nanofibers (ChNF) and anionic seaweed alginate (SA) is introduced for interfacial complexation to construct composite microfibers. The optimized condition to spin ChNF/SA is found by adjusting the process variables, including concentration of the components, pH, and the spinning rate. Dried ChNF-based microfibers revealed a core/shell morphology. The mechanical properties of ChNF/SA composite microfibers were determined as a function of ChNF aspect ratio, which was varied by controlling the mechanical deconstruction process of the precursor chitin. The obtained composite microfibers display the expected mechanical stability under humid conditions and offer functionalization opportunities, given the presence of both carboxylic and amino groups.

RESULTS AND DISCUSSION

Chitin nanofibers. We first demonstrate that the mechanical properties of the IPNC microfibers depend strongly on the aspect ratio of the precursor nanofibers. For this, partially deacetylated chitin, i.e., chitin nanofibers (ChNF) were produced to yield populations with three different average aspect ratios. This was achieved mainly by changing the mechanical deconstruction processes, as we reported recently.[12,13] More specifically, deacetylated chitin was disintegrated into ChNF by using microfluidization, followed by ultrasonication for given periods. The obtained chitin nanofibers were of high, medium and low aspect ratios, herein termed as ChNF-H, ChNF-M, ChNF-L, respectively (**Figure 1 bottom**). In more detail, the aspect ratio (length/width) of ChNF-M and ChNF-L corresponded to ~25 and ~15, respectively. ChNF-H presented a more complex morphology, but the axial aspect was estimated to be at least 60, much larger than those of ChNF-M and ChNF-L.

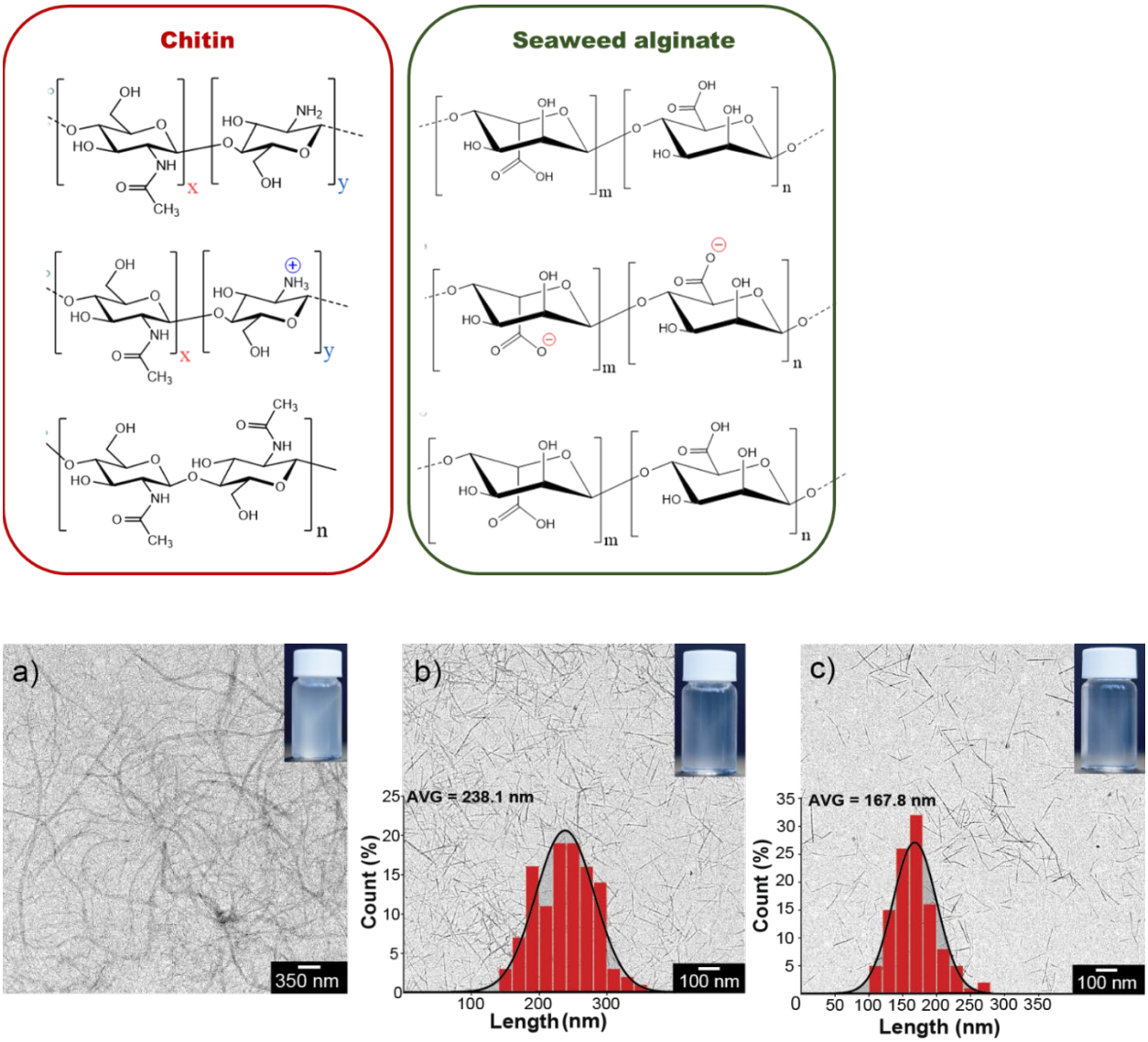

Figure 1. Top: Schematic illustration of the molecular formulae of partially deacetylated chitin derived from crab shells and seaweed alginate. Three possibilities are shown for the balance of charges. **Bottom**: TEM images of chitin nanofibers obtained from the hydrolysis of residual blue crab chitin followed by partial deacetylation and one pass microfluidization, yielding (a) chitin nanofibers of high aspect ratio (ChNF-H). By applying sonication to aqueous suspensions of ChNF-H, shorter nanofibers are obtained: nanofibers of (b) intermediate aspect ratio, CNF-M (25 min sonication), and (c) low aspect ratio, ChNF-L (50 min sonication). The insets in (b) and (c) correspond to histograms of the fibril axial size obtained by image analysis (at least 100 measurements). For ChNF-M and CHNF-L the respective length (and lateral size) are 267 ± 35 (11 ± 3 nm) and 168 ± 25 (11 ± 2 nm), respectively. The corresponding axial ratio (length/width)

is ~25 (ChNF-M) and ~15 (ChNF-L). Given the complex morphology of ChNF-H, it is difficult to report accurate values for length and width, however, they are estimated to be 2270 ± 1600 nm (39 ± 28 nm), yielding an aspect ratio ≥ 60, considerably larger than those of ChNF-M and ChNF-L.

Dry spinning. To generate ChNF/SA composite microfibers, droplets (~ 100 µL) of SA solution and ChNF suspensions were deposited next to each other on a hydrophobic surface (Teflon) (**Figure 2a**). Then, an inverted tweezer was used to bring the drops into contact; a complex was immediately formed at the interface, which prevented further fluid mixing (**Figure 2b**). The composite microfibers were produced by simply drawing from the interface (**Figure 2c** and **d**) until exhaustion of any of the two reservoirs (droplets) (see Supporting Information video). An alternative geometry is shown in ref[9]. The corresponding wet threads were then suspended and allowed to dry at room temperature, resulting in the composite microfibers. Previously, it was demonstrated that the selection of the concentration for the anionic solution and the cationic suspension is critical for the spinnability of the system.[9,11,14,15]

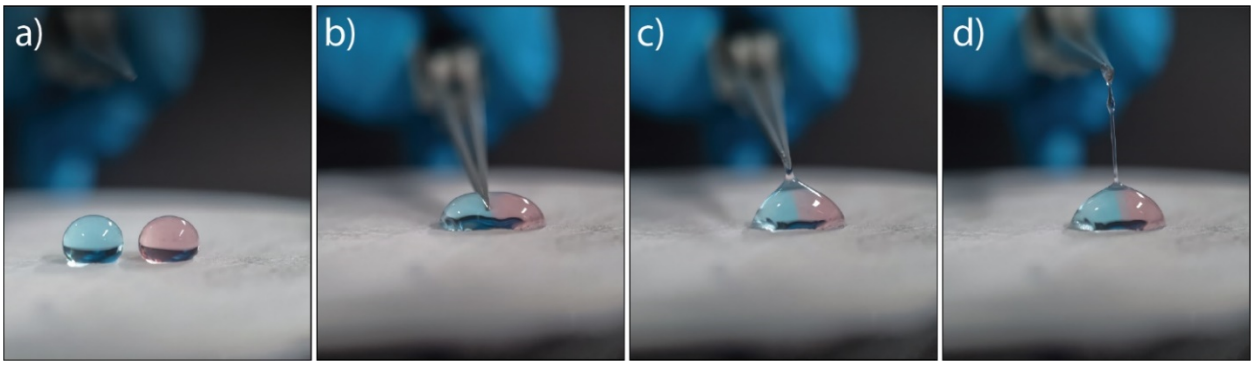

Figure 2. (a) Droplets of alginate solution (SA, blue) and chitin nanofiber suspension (ChNF, red) placed on a hydrophobic surface. (b) Upon droplet contact, a viscous interface is formed *via* interfacial polyelectrolyte-nanofiber complexation (IPNC). (c) Drawing of the viscous interface leads to dry spinning, which enables the formation of a (d) composite microfiber.

The concentrations of ChNF and SA were optimized for composite microfiber formation, corresponding to 0.3-0.4 wt% (ChNF) and 1 wt% (SA). Composite microfibers were easily formed with lengths (about 1 m) that were limited only by the available reservoir (drop) volume. Compared to ChNF-M and ChNF-L, microfibers based on ChNF-H allowed easier drawing of the interface to begin the spinning process even at low concentrations. This is reasonable, given that the larger aspect ratio of ChNF-H allows more effective complexation with anionic alginate polymers, analogical to the effect of molecular weight in the corresponding polyelectrolyte complexes.[16] However, it was interesting to note that the thread broke more frequently in the case of ChNF-H during the spinning process, which is likely a result of the stronger tendency for the larger nanofibers to form bundles that act as "defects", given their higher potential for crowding. As a microfiber was drawn from the liquid medium, a renewed interface was continuously formed by the electrostatic complexation upon replacement with fresh material through diffusion. Compared to ChNF-H, ChNF-M and ChNF-L formed thinner interfaces upon contact with SA and were more difficult to be draw. The impact of ChNF size and component concentrations on the microfiber diameter and spinnability is indicated in **Table S1** of the Supporting Information.

The driving force for the polyelectrolyte complexation from aqueous solution is a combination of the electrostatic interactions[17] and entropy changes, which stems from the release of counterions and water expulsion.[10,18,19] Inter-polyelectrolyte complexation usually occurs by association of highly diluted oppositely charged materials. The formation of a film at the interface involves the expulsion of water during the association of the charged components upon droplet contact. Previous works have demonstrated, through quartz crystal microbalance (QCM-D) and surface plasmon resonance (SPR), that cationic polymers adsorb and neutralize the surface charge of anionic cellulose films, resulting in water expulsion from the interfacial sites.[20,21] The observations

indicate the important role of water coupling to the adsorbed layer and the changes in hydration/swelling.

The interaction between macromolecules can be described as a function of free energy of binding (ΔG) which is related to the changes of enthalpy (ΔH) and entropy (ΔS), $\Delta G = \Delta H - T\Delta S$. Owing to the spontaneous formation of the complex, the free energy of binding shall be negative. Thus, a negative value is expected for the interaction between the components (ΔH) while $T\Delta S$ is highly positive. The release of the counterions, which depends on the electrolyte concentration, is responsible for the increase of the total entropy of the system. Therefore, the association of the components into a complex is driven by the counterion entropy.[22] However, the interaction between the macromolecular component, i.e., alginate and the chitin nanofiber is more challenging to rationalize. The IPNC involves a wide range of length scales, leading a competition of long-range Coulombic interactions and more localized interactions, such as ion pairing.[23–25] The release of counter ions, soon after interfacial contact, promotes binding between the components (**Figure S1**). Thus, the charge density and charge distribution have a critical role in determining the spinnability of the system into IPNC microfibers.[7]

The charge densities of SA and ChNF were examined by measuring the ζ -potential at different pH values (**Figure 3a**). ChNF dispersions exhibited positive ζ -potential values, and a zero net charge was approached as the pH became neutral. This is expected for chitin and chitosan, given the presence of primary amine groups, which become progressively protonated as the pH decreases to around 3.[26–28] Since the different aspect ratios were obtained from partially deacetylated chitin, ChNF-L, ChNF-M, ChNF-H exhibited similar positive ζ -potential profiles. SA was negatively charged in the whole range of pH tested, from pH 6 to 11; the deprotonation of carboxylic acid

groups in the polymer backbone resulted in a higher ζ -potential. The increase of the ζ –potential of SA going from pH 6 to pH 2 is related to polymer precipitation.

When both components were highly charged, ChNF at pH < 3.0 and SA at pH > 6, a strong complex was formed, making drawing difficult. ChNF/SA microfibers were easily drawn by using aqueous suspensions closer to neutral pH, for example, at pH 4 and 7 for ChNF and SA, respectively. Under such conditions, excessively strong complexation and flocs were avoided, which otherwise lead to inhomogeneities during spinning.

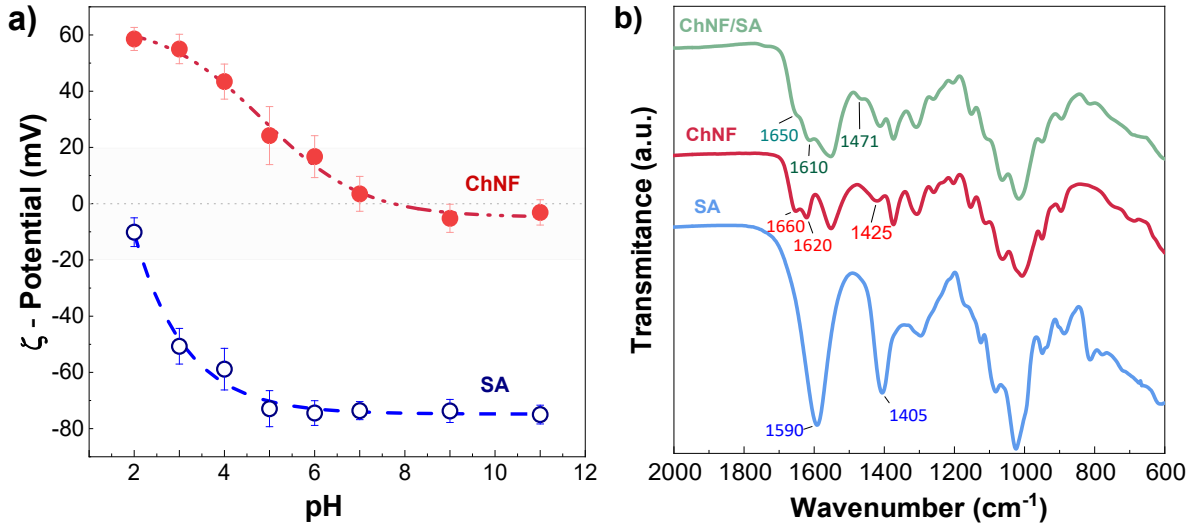

Figure 3. (a) ζ-potential of aqueous ChNF-H suspensions and SA solutions as a function of the respective pH. Optimal pH conditions for microfiber formation were found to be pH = 4 and 7 for ChNF and SA, respectively. Note: ChNF-L, ChNF-M, ChNF-H exhibited similar ζ -potential profiles. (b) FTIR spectra of pure SA, ChNF and dried composite microfibers of ChNF and SA.

Composition of the composite microfibers. The ChNF/SA chemical composition was determined by FTIR (**Figure 3b**). The characteristic absorption bands related to alginate are found at 1590 and 1405 cm^{-1}, related to the carboxyl anion stretching and at 1296 cm^{-1} assigned to the backbone vibration.[26] ChNF spectra showed amine groups from partial deacetylation, which overlapped with the peaks of alginate at 1660 and 1610 cm^{-1} (amide-I) and 1550 cm^{-1} (amide-

II).[29,30] Note that the spectrum corresponding to the ChNF/SA composite microfiber followed closely that of pure ChNF, suggesting the dominant presence ChNF in the composite microfibers. This is supported by elemental analysis (**Table S2**) and titration (**Figure S2**). Moreover, some differences in the composite (ChNF/SA) spectra were noted compared to those of the single ChNF and SA components. The amide-I bands showed a broader shoulder at 1650 and 1610 cm^{-1}, whereas amide-II was observed as broader absorption band at 1550 cm^{-1}. On the other hand, the fingerprint of carboxylic groups ($–COO^-$) on sodium alginate disappeared, previously observed at 1590 cm^{-1}, suggesting an electrostatic association with the positively charged amino groups ($–NH_3^+$) of ChNF. This is in agreement with the reported association between SA and chitosan.[31–34]

Composite microfiber morphology. We investigated the morphology of the dried composite microfibers using SEM, **Figure 4.** Generally, the composite microfibers obtained from all ChNF types (ChNF-H, ChNF-M and ChNF-L) displayed a similar morphology. Thus, the following discussion refers to ChNF-H/SA, as representative for the other two cases. In general, the ChNF/SA composite microfibers showed homogenous diameters along the length (**Figure 4a**). The texture of the microfiber surface (**Figure 4b** and **4c)** were dominated by veining/nervation patterns.[7,9–11,35–38] Moreover, there was evidence of a hierarchical structure, as found in previous works.[9–11,14] Therein, the components are organized by sub-units wherein macromolecules bind during the complexation as "nucleation sites" and spread closely to the interfaces. The nucleation sites grow to form several fibrous units and pack together during the drawing process, forming submicron fibrils (microfibrils), which are align parallel and merge along the length, giving rise to the thread itself. The irregularity on the packings results in vein patterns. Recently, a hierarchical assembly was also observed in complex fibers by using nanofibers of opposite charges.[11] It is interesting to note that the resultant fibers were assembled hierarchically, bearing little influence

from the identity of the components, whether macromolecules or nanofibers, as was also demonstrated by the complexation of highly charged TEMPO-oxidized cellulose nanofibers (TOCN)[9,10] As a further reference, we performed experiments with TOCN and ChNF, which led to successful dry spinning and to the formation of composite microfibers (**Figure S3**).

The nature of the vein pattern formed on the surface of the microfibers is intriguing and prompted more detailed studies. For instance, the surface of the microfibers was observed to be fully covered with fibrils that were distributed random (**Figure 4d,e**). The morphology of such fibrils is similar to that of individual chitin nanofibers (**Figure 1**), but present a significantly wider lateral dimension, indicating ChNF associated with SA where the average diameter of individual ChNF is 3 ± 2 nm, whereas the structures shown on the microfibers are considerably thicker, 8 ± 3 nm. Thus, it is reasonable to expect that cationic ChNF is covered by a sleeve of anionic SA formed during complexation besides the platinum coat that were deposited for SEM sample preparation.

The core or center of the microfibers was accessed by cryo-fracturing (**Figure 4f**, **g**, and **h**). A circular cross-section (**Figure 4f**) is revealed, with clear evidence of aligned microfibrils, which are bound into compact structures. The finer fibrous units appeared as parallel “spikes” distributed throughout the cross-sectional surface, indicating an orientation that aligned with the drawing (axial) direction.

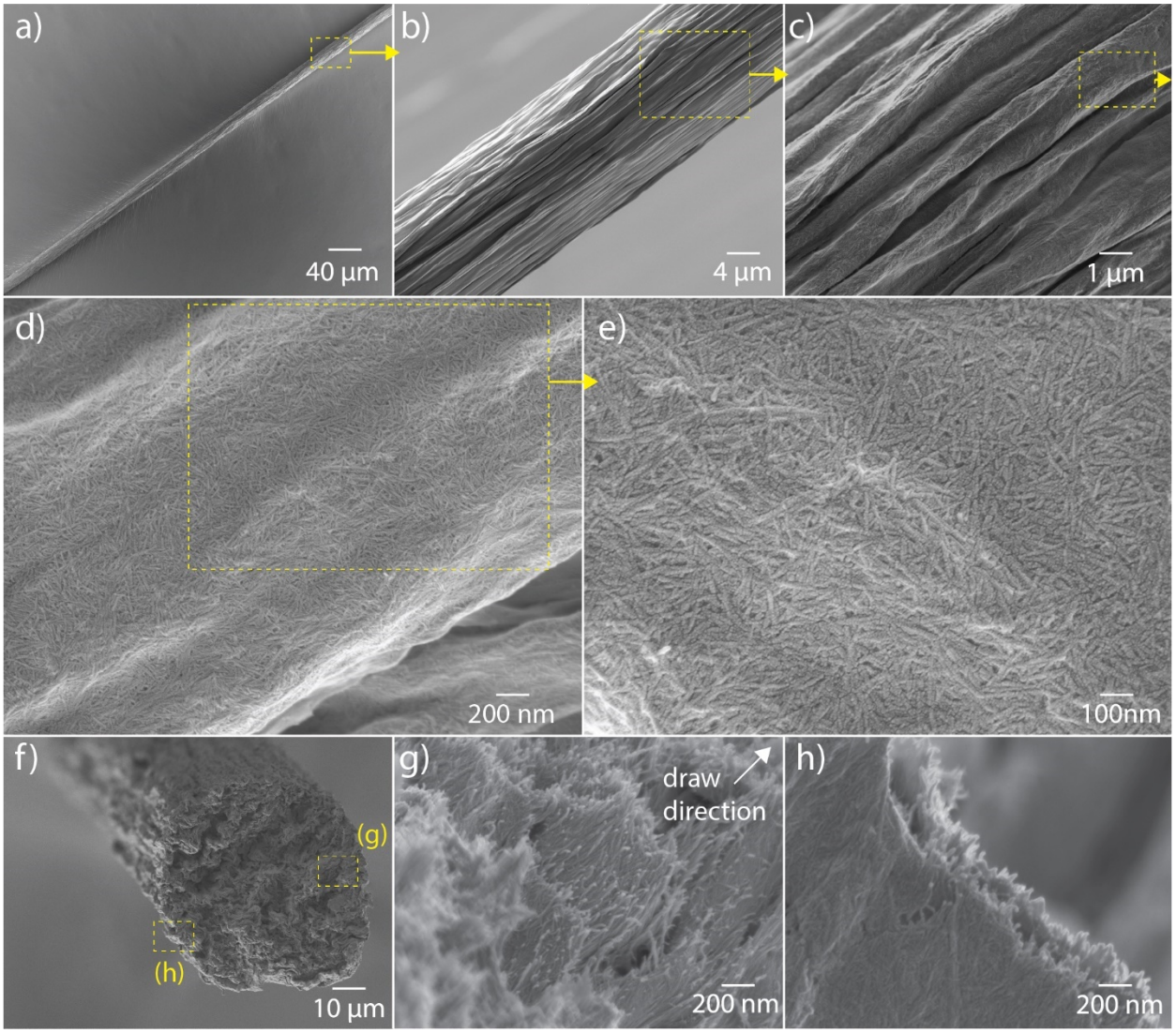

Figure 4. Low magnification SEM image of (a) dried ChNF-H/SA composite microfiber. The surface of the ChNF/SA composite microfiber is shown with higher magnifications (b and c) and displayed aligned vein structures. (d,e) Observation at even higher magnifications reveal randomly oriented fibrous units on the surface. (f) Cross sectional observation after cryo-fracture allows observation of the core of the microfibers in the (g) center and (h) shell. There is indication of alignment of ChNF inside the microfibers.

The observations support a core-shell structure in the composite microfibers, which has also been proposed for complexation with oppositely charged polyelectrolytes and nanofibers.[5,9,25,36,37,39] Based on our observations, it is reasonable to conclude that composite microfibers comprise a interfacial complex layer that is constantly formed by replenishment of the components at the interface upon drawing. Simultaneously, chitin nanofibers become covered by a sleeve of alginate and are oriented and packed along the formed microfiber axis by shear stress. As the wet microfiber is pulled from the liquid-liquid interface, complexes present in the fluid phase adsorb on its surface via hydrophilic or capillary effects. Such structures display limited or no alignment, thereby resulting in a random orientation on the microfiber surface, as shown in **Figure 4d, 4e**. IPNC dry spinning could be considered as a bottom-up process where the nanofibers, dispersed in aqueous medium, are spontaneously and continuously assembled into ordered supra-structures.

An interesting feature of the ChNF/SA system is associated with the bending flexibility of the composite microfibers, which can be easily tied into knots by hand (**Figure 5a**) or twisted (**Figure 5b**). In order to obtain a longitudinal fracture, a large stress was applied, tightening the knots, and causing delamination of the microfibers, which allowed observation of the internal morphology along the composite fiber length (**Figure 5c**). The ChNF/SA composite fiber showed a compact structure that was supported by the longitudinal fracture images, which revealed that the microfibers were composed of densely packed, smaller structures well aligned in the direction of drawing. The alignment of the sub-units, previously observed by the cross-sectional images, is more clearly seen in these images (**Figure 5d, 5e, 5f**).

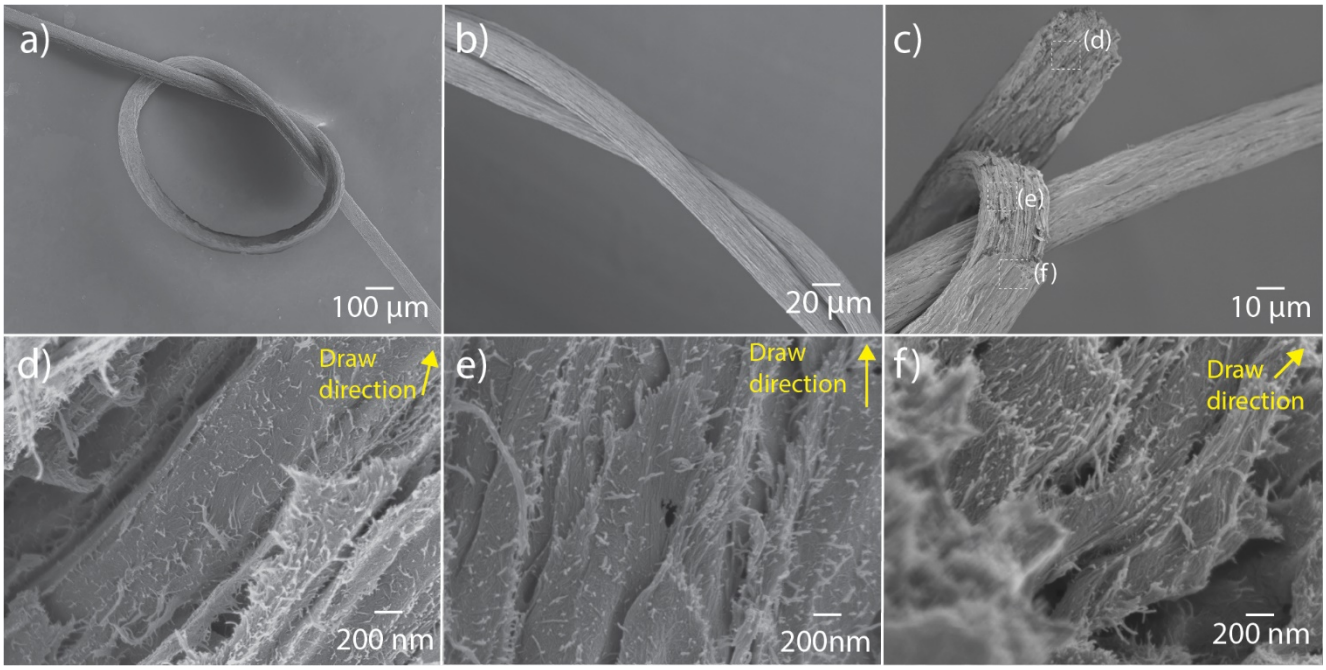

Figure 5. SEM images of (a) ChNF/SA composite microfiber tied as a knot. (b) Two composite microfibers twisted onto each other. In (c), one of the fibers was forced to rupture along the axis, revealing details of the inner areas, as shown in (d, e, f) for magnified sections displaying nanofiber orientation along with the drawing direction.

Fibril orientation in the spun microfibers. As observed in SEM imaging (**Figure 5**), the chitin fibrils tend to align in the axial direction, likely as a result from the drawing process. This is also supported by wide angle X-ray scattering (WAXS) data as suggested by the arcs of fiber reflection rings in the diffractograms of **Figure 6a**, and the peaks at 90 and 270 degrees from azimuthal profiles (**Figure 6b**). The orientation index as well as Herman's parameter were calculated to quantify the degree of orientation ("0" indicates a completely random structure and "1" reveals a fully oriented construction). A clear difference can be noticed from both indices: fibers made from fibrils with the highest aspect ratio (ChNF-H/SA), possess the highest orientation index (0.75) and Herman's parameter (0.56). The corresponding values for ChNF-M/SA are 0.73 and 0.44, respectively. ChNF-L/SA is poorly oriented (0.21 and 0.36, respectively). Thus, it is

clear that the aspect ratio significantly influences nanochitin alignment during spinning. These results are consistent with the fiber mechanical performance, as discussed next.

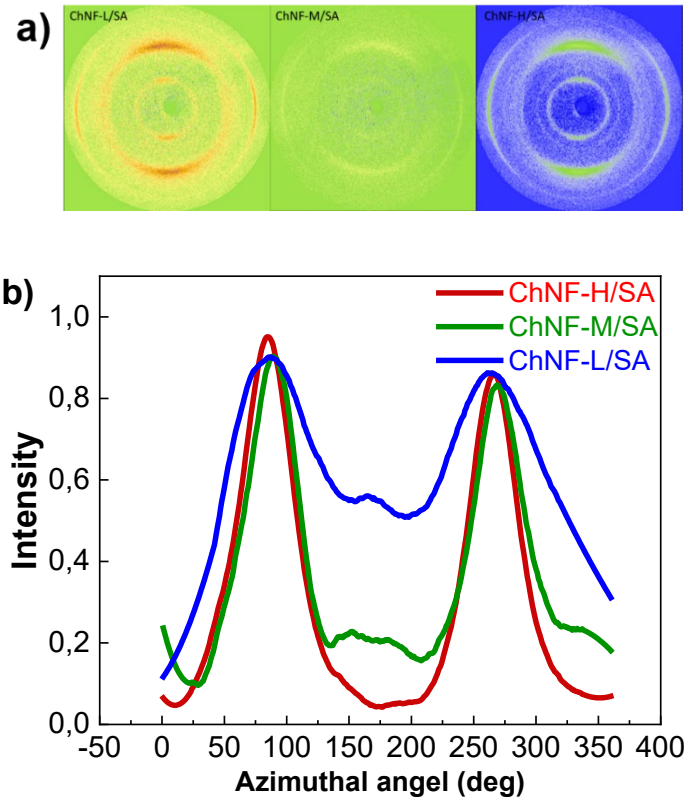

Figure 6. (a) WAXS diffractograms of ChNF/SA fibers, from left to right: ChNF-L/SA, ChNF-M/SA, ChNF-H/SA. (b) The respective azimuthal profiles obtained from (100) plane of the diffractograms.

Composite microfiber strength. To determine the mechanical properties of the microfibers, particularly the wet strength, tensile tests were carried at a relative humidity of 50% and upon immersion in water. Single microfibers were used for this purpose (1 wt% SA, 0.3 wt% ChNF drawn at a given drawing rate). In general, the mechanical strength of the composite ChNF/SA microfibers exhibited a mechanical strength comparable to that measured for filaments produced by wet spinning of single component, ChNF .[40,41]

A reduction in ChNF aspect ratio leads to a slight reduction in the Young's modulus and ultimate tensile strength, while the elongation at break is increased. Besides the lower orientation (WAXS), this is likely due to the more limited macromolecular entanglement in the presence of shorter nanoparticles, as has been also found in reinforced nanocomposites. A similar trend is observed for tensile tests carried out in water, as shown by the dashed lines in **Figure 7a.** The strong binding between ChNF and SA in the composite microfiber leads to robust microfibers that indicate promoted stability in water. Some plasticization is observed via water sorption, given the hydrophilic nature of the components. The inelastic behavior, noticed as a quasi-linear stress-stain curve, can be explained by the disentanglement of the interfibrillar/intermolecular hydrogen bonding. The weakening of these bonds produce sliding between the macromolecules and ChNF nanoparticles, resulting in an increase in the strain-to-failure up to 25% (ChNF-L) and 35% (ChNF-H). The values of the Young's modulus, ultimate tensile strength, and strain at break of the tested composite microfibers are listed in **Table S3**

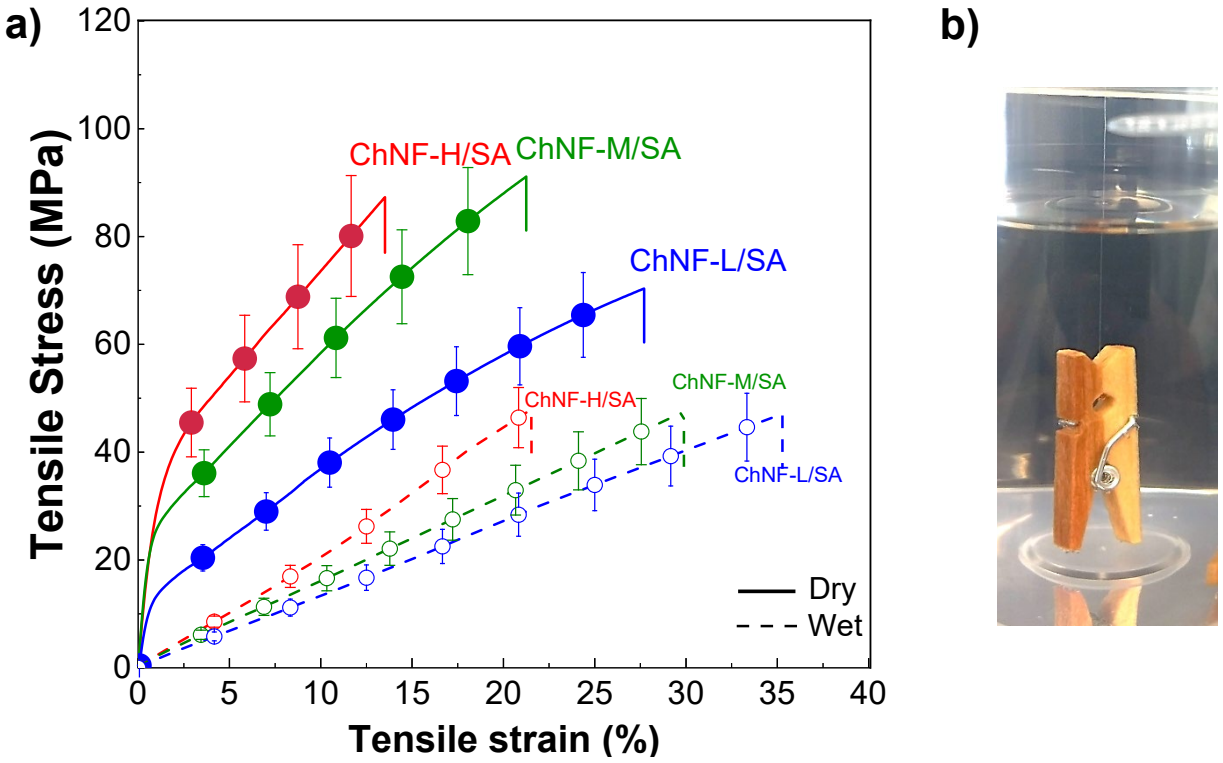

Figure 7. (a) Tensile tests for composite microfibers produced from ChNF-H, ChNF-M, and ChNF-L in dry and wet condition. The results, corresponding to microfibers containing about 40% alginate, in the absence of chemical crosslinking, are similar to those recorded for filaments obtained by wet spinning of single component ChNF. (**b)** Illustration of the wet strength of the microfibers.

It can be concluded that the mechanical properties of microfibers obtained by interfacial complexation are affected not only by the process parameters (e.g., drawing rate and component concentrations)[6,9,11,14,42], but also by the morphology of ChNF. Furthermore, ChNF/SA microfibers are highly stretchable when immersed in the aqueous medium. Tailoring the particles size should be evaluated in future studies to further improve the mechanical properties of the developed microfibers.[40]

CONCLUSIONS

We show that chitin nanofibers can be electrostatically complexed with sodium alginate to generate microfibers *via* a spontaneous interfacial polyelectrolyte-nanofiber complexation. The spinnability of the system is related to the complex formed at the interface of the media upon contact of the oppositely charged components. Parameters such as component concentration, pH and nanoparticle axial aspect can be tailored to enable microfiber drawing. The ChNF/SA microfibers exhibit a core/shell structure with distinct morphologies. The shell contains randomly oriented fibrous units formed by ChNFs coated by a sleeve of SA. The core, however, shows a hierarchical structure comprising nanofibers aligned in the longitudinal direction. Our findings contribute to further understand microfiber assembly during dry spinning. We demonstrate that the aspect ratio of the precursor nanofibers strongly affects the mechanical properties of the IPNC microfibers. ChNF/SA from high aspect ratio nanofibers exhibited the highest values in Young's modulus and tensile strength. They also exhibited a high wet strength, in spite the highly hydrophilic nature of the components.

EXPERIMENTAL SECTON

Materials. Partially deacetylated chitin nanofibers (ChNF) were prepared from mechanical methods as reported in literature[12]. Briefly, chitin from crab shells was treated in 33 wt% NaOH solution at 90 °C for 3.5 h. The liquid-to-solid ratio was 25 ml/g. This process results in partial deacetylation of the acetyl groups in chitin (de-chitin). Then, the residual solids were thoroughly washed with distilled water to remove the NaOH until reaching neutral pH. For nanofibrillation, deacetylated chitin was re-dispersed in MQ water at a concentration of 0.2 wt%, following by pH adjustment (3.0) with acetic acid under vigorous stirring. Then, the obtained coarse suspension was homogenized using a high-speed blender (T-25 Ultra-Turrax Digital Homogenizer, IKA, Germany) at room temperature. The disintegration of deacetylated chitin into ChNF can be achieved by two approaches: ultra-sonication and microfluidization. Ultra-sonication was performed using a titanium tip sonicator (Sonifier 450, Branson Ultrasonics Co., Danbury, CT, USA) at 50% amplitude with alternating on-off cycles (5 s - 2 s, respectively). 25 and 50 min sonication duration was used to produce nanofibers with different aspect ratios.[13] The nanofibrillated chitin suspension was then centrifuged at 10,000 rpm for 5 min to remove large particles, and the transparent supernatant was collected as ChNF. Microfluidization was carried out with a microfluidizer (M-110P, Microfluidics In, Newton, MA, USA) through one pass at a pressure of 1,500 bar. Microfluidization, and the sonication at 25 min and 50 min resulted in high, medium and low aspect ratio, respectively, which was denoted as ChNF-H, ChNF-M, ChNF-L. The deacetylation degree determined by conductometric titration was approximately ~25%.

Sodium alginate (SA), medium molecular weight (W201502), was purchased from Sigma-Aldrich. SA was dissolved in 100 ml of deionized water to obtain 1 wt %. The resulting solution

was stirred with a magnetic stirrer for 24h. Then, the SA solution was filtrated to remove any remaining insoluble aggregates and impurities.

ChNF aspect ratio. By processing the ChNF TEM images using ImageJ software, it was found that the average length and width of ChNF-L were 168 ± 25 and 11 ± 2 nm, respectively. ChNF-M showed respective values of 267 ± 35 and 11 ± 3 nm. Thus, the corresponding axial ratio (length/width) was ~15 to ChNF-L and ~25 to ChNF-M. Given the complex morphology of ChNF-H, it was difficult to accurately measure the length and width of individual nanoparticles in this sample. However, on the basis of ChNF-H and bundles identified from TEM micrographs, an average width and length of 39 ± 28 nm and 2270 ± 1600 nm were obtained (based on 100 measurements from ImageJ). Thus, it can be estimated that the axial ratio for ChNF-H was ≥ 60, much larger than those of ChNF-M and ChNF-L. Admittedly, the actual axial ratio of ChNF-H in suspension might vary significantly due to the existence of irregular bundles. The obtained aspect ratio values are corroborated by a recent report where chitin suspensions were prepared following the same conditions used here.[13,43]

IPNC spinning of ChNF/SA. 100 μL droplets of ChNF and SA were placed near each other in a Teflon plate. Then, using an inverted tweezer, the droplets were cautiously brought into contact. At this stage, it can be visually observed a thin film ensuing at the interface, preventing further mixture of the liquids. The interface that was the locus in with the tweezers was plunged to grab the membrane and dragged vertically resulting in the continuous microfiber spinning process. The most of microfibers produced from hand drawing showed homogeneous surface along all the microfiber direction. However, previous work has shown that regular beads (defects) are formed in IPC microfibers depending on the drawing rate, which can compromise the mechanical integrity.[14] Thus, an automatic roller was used as a collector for better controlling the

spinning rate. The microfibers used in mechanical tests were obtained at constant spinning velocity of 30 mm/s. Under appropriated conditions, 90 cm long microfibers could be obtained by spinning it from a pair of 100 μm droplets.

Zeta potential. To obtain qualitative data about the surface charge of cationic sodium alginate and anionic ChNF, zeta potential (ζ-potential) were performed by a Zetasizer Nano ZS90 (Malvern Instruments). The pH (2-11) for SA and ChNF was adjusted using 1 M, 0.5 M and 0.1 M HCl or NaOH. All the measurements were performed with triplicate and reported as an average with standard deviations.

Fourier Transform Infrared (FTIR) Spectroscopy. FTIR spectra were acquired using a Nicolet 380 Spectrometer (Nicolet Instrument Co., Madison, USA) equipped with smart orbit single reflection diamond ATR from 32 scans for all experiments. The raw materials and the corresponding microfibers were first dried prior testing.

Scanning Electron Microscopy (SEM). SEM images of ChNF/SA microfibers were obtained by a Zeiss Sigma VP scanning electron microscope. Images from the surface of the microfibers were obtained from samples attached to aluminum stubs by just using carbon tape. Cross-section images were obtained by fracturing ChNF/SA microfibers in liquid nitrogen and then attach the microfiber to the stub. All the samples were sputter coated with a platinum layer of 4 nm thick.

Wide angle X-ray scattering (WAXS). The orientation of chitin crystallites was determined by WAXS. Sample diffraction images were collected from transmission geometry at a wavelength of 1.54 Å using a MicroMax-007 HF X-ray generator (Rigaku, Japan). A bundle of fiber were aligned horizontally and placed perpendicular to the beam (120 μm size) using a exposure time of 10 minutes and 300 mm distance to detector (Mar345 imaging plate detector). Azimuthal intensity distribution profiles were obtained from (100) peak after subtracting the background, based on

which the orientation index (π) and Herman's orientation parameter (S) were calculated according to equations (1) and (2).[44]

$$\pi = \frac{180^{\circ} - FWHM}{180^{\circ}} \qquad (1)$$

where FWHM is the full width at the half maximum (in degrees) of one of the two peaks in the azimuthal intensity distribution profile. π was calculated for both peaks and their average reported.

$$S = \frac{3}{2} < cos^2\gamma > -\frac{1}{2} \qquad (2)$$

Assuming cylindrical symmetry in the filament, the average cosine *‹cos²γ›* was obtained from the average cosine of the azimuthal angle *φ* according to equation (3).

$$\langle cos^2\gamma \rangle = 1 - 2\langle cos^2\varphi \rangle \qquad (3)$$

where

$$< cos^2\varphi >= \frac{\sum_{\varphi_0}^{\varphi_0 + \pi/2} I(\varphi) \sin\varphi \, cos^2\varphi}{\sum_{\varphi_0}^{\varphi_0 + \pi/2} I(\varphi) \sin\varphi}$$

Here *I(φ)* is the intensity detected at azimuthal angle *φ,* and φ_0 is the azimuthal angle in the beginning of the range used for the calculation of the average cosine *‹cos²φ›. S* was calculated at φ_0 of 0, π/2, π and 3π/2 and the average of these values is reported.

Mechanical tests. Specimens to tensile tests were prepared cutting the ChNF/SA microfibers in 2 cm long and glued the ends to a paper frame of (20 mm x 5 mm), leaving a testing window of 10 mm x 3 mm. Window frame was used to help attach the samples to the clamps, and prevent slippage and stretch prior to testing. ChNF/SA microfibers were conditioned 48 h at 24 °C and 50% humidity relativity room prior testing. The specimens were stretched at 2 mm/s until fracture, using a single-column universal tester Instron 5944 equipped with 5kN load cell. Six specimens

of each sample were tested, and the diameter of the samples were measured by optical/SEM microscopy. Typically, the microfiber's diameter tested was around 40 µm, and the cross section was assumed to be circular, which was supported by SEM images (**Figure 4f**).

The influence of water on the tensile behavior of the ChNF/SA microfibers was evaluated by testing these materials under water. Wet tensile testing was performed on FAVIGRAPH semiautomatic equipment (Textechno Company, Germany) with 100-mm long microfibers that were attached to the clamps. Then, the specimen was plunged into water by 30s followed by stretching at 2 mm/s until fracture.

ASSOCIATED CONTENT

Supporting information. Supporting information is accessible online free of charge. It consist of a video about the interfacial complexation, a schematic illustration of the interactions upon interfacial complexation; a table with the effect of ChNF aspect ratio and concentration of SA and ChNF on fiber spinnability and microfiber diameter; elemental analysis of ChNF/SA fibers obtained from different aspect ratios; zeta potential of sodium alginate in ChNF suspension; SEM images of the surface of ChNF/TOCN microfibers; mechanical properties of ChNF/SA microfibers obtained from ChNF of different aspect ratio

AUTHOR INFORMATION

*E-mail – Orlando.rojas@aalto.if (O.J.R.), Tel: +358-(0)50 512 4227;

*E-mail – rafaelgrandee@gmail.com (G. R.) Tel +358-(041

Author Contributions

The manuscript was written through contributions of all authors. All authors have given approval to the final version of the manuscript

REFERENCES

(1) Islam, S.; Bhuiyan, M. A. R.; Islam, M. N. Chitin and Chitosan: Structure, Properties and Applications in Biomedical Engineering. *J. Polym. Environ.* **2017**, *25* (3), 854–866. https://doi.org/10.1007/s10924-016-0865-5.

(2) Shamshina, J. L.; Gurau, G.; Block, L. E.; Hansen, L. K.; Dingee, C.; Walters, A.; Rogers, R. D. Chitin–Calcium Alginate Composite Fibers for Wound Care Dressings Spun from Ionic Liquid Solution. *J. Mater. Chem. B* **2014**, *2* (25), 3924–3936. https://doi.org/10.1039/C4TB00329B.

(3) Jayakumar, R.; Prabaharan, M.; Sudheesh Kumar, P. T.; Nair, S. V.; Tamura, H. Biomaterials Based on Chitin and Chitosan in Wound Dressing Applications. *Biotechnol. Adv.* **2011**, *29* (3), 322–337. https://doi.org/10.1016/j.biotechadv.2011.01.005.

(4) Dai, T.; Tanaka, M.; Huang, Y.-Y.; Hamblin, M. R. Chitosan Preparations for Wounds and Burns: Antimicrobial and Wound-Healing Effects. *Expert Rev. Anti. Infect. Ther.* **2011**, *9* (7), 857–879. https://doi.org/10.1586/eri.11.59.

(5) Amaike, M.; Senoo, Y.; Yamamoto, H. Sphere, Honeycomb, Regularly Spaced Droplet and Fiber Structures of Polyion Complexes of Chitosan and Gellan. *Macromol. Rapid Commun.* **1998**, *19* (6), 287–289. https://doi.org/10.1002/(SICI)1521-3927(19980601)19:6<287::AID-MARC287>3.3.CO;2-O.

(6) Huang, W.; Liu, D.; Li, J.; Zhu, L.; Yang, S. Polymer Complexation for Functional Fibers. *Sci. China Technol. Sci.* **2019**, *62* (6), 931–944. https://doi.org/10.1007/s11431-018-9475-5.

(7) Wan, A. C. A.; Cutiongco, M. F. A.; Tai, B. C. U.; Leong, M. F.; Lu, H. F.; Yim, E. K. F. Fibers by Interfacial Polyelectrolyte Complexation – Processes, Materials and Applications.

Mater. Today **2016**, *19* (8), 437–450. https://doi.org/10.1016/j.mattod.2016.01.017.

(8) Zou, J.; Kim, F. Self-Assembly of Two-Dimensional Nanosheets Induced by Interfacial Polyionic Complexation. *ACS Nano* **2012**, *6* (12), 10606–10613. https://doi.org/10.1021/nn303608g.

(9) Toivonen, M. S.; Kurki-Suonio, S.; Wagermaier, W.; Hynninen, V.; Hietala, S.; Ikkala, O. Interfacial Polyelectrolyte Complex Spinning of Cellulose Nanofibrils for Advanced Bicomponent Fibers. *Biomacromolecules* **2017**, *18* (4), 1293–1301. https://doi.org/10.1021/acs.biomac.7b00059.

(10) Grande, R.; Trovatti, E.; Carvalho, A. J. F.; Gandini, A. Continuous Microfiber Drawing by Interfacial Charge Complexation between Anionic Cellulose Nanofibers and Cationic Chitosan. *J. Mater. Chem. A* **2017**, *5* (25), 13098–13103. https://doi.org/10.1039/C7TA02467C.

(11) Zhang, K.; Liimatainen, H. Hierarchical Assembly of Nanocellulose-Based Filaments by Interfacial Complexation. *Small* **2018**, *14* (38), 1801937. https://doi.org/10.1002/smll.201801937.

(12) Fan, Y.; Fukuzumi, H.; Saito, T.; Isogai, A. Comparative Characterization of Aqueous Dispersions and Cast Films of Different Chitin Nanowhiskers/Nanofibers. *Int. J. Biol. Macromol.* **2012**, *50* (1), 69–76. https://doi.org/10.1016/j.ijbiomac.2011.09.026.

(13) Bai, L.; Huan, S.; Xiang, W.; Liu, L.; Yang, Y.; Nugroho, R. W. N.; Fan, Y.; Rojas, O. J. Self-Assembled Networks of Short and Long Chitin Nanoparticles for Oil/Water Interfacial Superstabilization. *ACS Sustain. Chem. Eng.* **2019**, *7* (7), 6497–6511. https://doi.org/10.1021/acssuschemeng.8b04023.

(14) Wan, A. C. A.; Liao, I.-C.; Yim, E. K. F.; Leong, K. W. Mechanism of Fiber Formation by Interfacial Polyelectrolyte Complexation. *Macromolecules* **2004**, *37* (18), 7019–7025. https://doi.org/10.1021/ma0498868.

(15) Mendes, A. C.; Strohmenger, T.; Goycoolea, F.; Chronakis, I. S. Electrostatic Self-Assembly of Polysaccharides into Nanofibers. *Colloids Surfaces A Physicochem. Eng. Asp.*

2017, *531*, 182–188. https://doi.org/10.1016/j.colsurfa.2017.07.044.

(16) Sæther, H. V.; Holme, H. K.; Maurstad, G.; Smidsrød, O.; Stokke, B. T. Polyelectrolyte Complex Formation Using Alginate and Chitosan. *Carbohydr. Polym.* **2008**, *74* (4), 813–821. https://doi.org/10.1016/j.carbpol.2008.04.048.

(17) Wang, F.; Liu, Z.; Wang, B.; Feng, L.; Liu, L.; Lv, F.; Wang, Y.; Wang, S. Multi-Colored Fibers by Self-Assembly of DNA, Histone Proteins, and Cationic Conjugated Polymers. *Angew. Chemie Int. Ed.* **2014**, *53* (2), 424–428. https://doi.org/10.1002/anie.201308795.

(18) Shamoun, R. F.; Reisch, A.; Schlenoff, J. B. Extruded Saloplastic Polyelectrolyte Complexes. *Adv. Funct. Mater.* **2012**, *22* (9), 1923–1931. https://doi.org/10.1002/adfm.201102787.

(19) Meka, V. S.; Sing, M. K. G.; Pichika, M. R.; Nali, S. R.; Kolapalli, V. R. M.; Kesharwani, P. A Comprehensive Review on Polyelectrolyte Complexes. *Drug Discov. Today* **2017**, *22* (11), 1697–1706. https://doi.org/10.1016/j.drudis.2017.06.008.

(20) Vuoriluoto, M.; Orelma, H.; Johansson, L.-S.; Zhu, B.; Poutanen, M.; Walther, A.; Laine, J.; Rojas, O. J. Effect of Molecular Architecture of PDMAEMA–POEGMA Random and Block Copolymers on Their Adsorption on Regenerated and Anionic Nanocelluloses and Evidence of Interfacial Water Expulsion. *J. Phys. Chem. B* **2015**, *119* (49), 15275–15286. https://doi.org/10.1021/acs.jpcb.5b07628.

(21) Orelma, H.; Filpponen, I.; Johansson, L.-S.; Laine, J.; Rojas, O. J. Modification of Cellulose Films by Adsorption of CMC and Chitosan for Controlled Attachment of Biomolecules. *Biomacromolecules* **2011**, *12* (12), 4311–4318. https://doi.org/10.1021/bm201236a.

(22) Fu, J.; Schlenoff, J. B. Driving Forces for Oppositely Charged Polyion Association in Aqueous Solutions: Enthalpic, Entropic, but Not Electrostatic. *J. Am. Chem. Soc.* **2016**, *138* (3), 980–990. https://doi.org/10.1021/jacs.5b11878.

(23) Sing, C. E. Development of the Modern Theory of Polymeric Complex Coacervation. *Adv. Colloid Interface Sci.* **2017**, *239*, 2–16. https://doi.org/10.1016/j.cis.2016.04.004.

(24) Fu, J.; Fares, H. M.; Schlenoff, J. B. Ion-Pairing Strength in Polyelectrolyte Complexes.

Macromolecules **2017**, *50* (3), 1066–1074. https://doi.org/10.1021/acs.macromol.6b02445.

(25) Ohkawa, K.; Kitagawa, T.; Yamamoto, H. Preparation and Characterization of Chitosan-Gellan Hybrid Capsules Formed by Self-Assembly at an Aqueous Solution Interface. *Macromol. Mater. Eng.* **2004**, *289* (1), 33–40. https://doi.org/10.1002/mame.200300188.

(26) Li, X.; Xie, H.; Lin, J.; Xie, W.; Ma, X. Characterization and Biodegradation of Chitosan–Alginate Polyelectrolyte Complexes. *Polym. Degrad. Stab.* **2009**, *94* (1), 1–6. https://doi.org/10.1016/j.polymdegradstab.2008.10.017.

(27) Berger, J.; Reist, M.; Mayer, J. M.; Felt, O.; Peppas, N. A.; Gurny, R. Structure and Interactions in Covalently and Ionically Crosslinked Chitosan Hydrogels for Biomedical Applications. *Eur. J. Pharm. Biopharm.* **2004**, *57* (1), 19–34. https://doi.org/10.1016/S0939-6411(03)00161-9.

(28) Ravi Kumar, M. N. . A Review of Chitin and Chitosan Applications. *React. Funct. Polym.* **2000**, *46* (1), 1–27. https://doi.org/10.1016/S1381-5148(00)00038-9.

(29) Ifuku, S.; Nogi, M.; Abe, K.; Yoshioka, M.; Morimoto, M.; Saimoto, H.; Yano, H. Preparation of Chitin Nanofibers with a Uniform Width as α-Chitin from Crab Shells. *Biomacromolecules* **2009**, *10* (6), 1584–1588. https://doi.org/10.1021/bm900163d.

(30) Li, M.-C.; Wu, Q.; Song, K.; Cheng, H. N.; Suzuki, S.; Lei, T. Chitin Nanofibers as Reinforcing and Antimicrobial Agents in Carboxymethyl Cellulose Films: Influence of Partial Deacetylation. *ACS Sustain. Chem. Eng.* **2016**, *4* (8), 4385–4395. https://doi.org/10.1021/acssuschemeng.6b00981.

(31) Lawrie, G.; Keen, I.; Drew, B.; Chandler-Temple, A.; Rintoul, L.; Fredericks, P.; Grøndahl, L. Interactions between Alginate and Chitosan Biopolymers Characterized Using FTIR and XPS. *Biomacromolecules* **2007**, *8* (8), 2533–2541. https://doi.org/10.1021/bm070014y.

(32) Li, Z.; Ramay, H. R.; Hauch, K. D.; Xiao, D.; Zhang, M. Chitosan–Alginate Hybrid Scaffolds for Bone Tissue Engineering. *Biomaterials* **2005**, *26* (18), 3919–3928. https://doi.org/10.1016/j.biomaterials.2004.09.062.

(33) Smitha, B.; Sridhar, S.; Khan, A. A. Chitosan–Sodium Alginate Polyion Complexes as Fuel

Cell Membranes. *Eur. Polym. J.* **2005**, *41* (8), 1859–1866. https://doi.org/10.1016/j.eurpolymj.2005.02.018.

(34) Simsek-Ege, F. A.; Bond, G. M.; Stringer, J. Polyelectrolyte Complex Formation between Alginate and Chitosan as a Function of PH. *J. Appl. Polym. Sci.* **2003**, *88* (2), 346–351. https://doi.org/10.1002/app.11989.

(35) Carretero, A.; Soares da Costa, D.; Reis, R. L.; Pashkuleva, I. Extracellular Matrix-Inspired Assembly of Glycosaminoglycan–Collagen Fibers. *J. Mater. Chem. B* **2017**, *5* (17), 3103–3106. https://doi.org/10.1039/C7TB00704C.

(36) Ohkawa, K.; Takahashi, Y.; Yamada, M.; Yamamoto, H. Polyion Complex Fiber and Capsule Formed by Self-Assembly of Chitosan and Poly(α,L-Glutamic Acid) at Solution Interfaces. *Macromol. Mater. Eng.* **2001**, *286* (3), 168–175. https://doi.org/10.1002/1439-2054(20010301)286:3<168::AID-MAME168>3.0.CO;2-7.

(37) Yamamoto, H.; Senoo, Y. Polyion Complex Fiber and Capsule Formed by Self-Assembly of Chitosan and Gellan at Solution Interfaces. *Macromol. Chem. Phys.* **2000**, *201* (1), 84–92. https://doi.org/10.1002/(SICI)1521-3935(20000101)201:1<84::AID-MACP84>3.0.CO;2-Y.

(38) Nechyporchuk, O.; Bordes, R.; Köhnke, T. Wet Spinning of Flame-Retardant Cellulosic Fibers Supported by Interfacial Complexation of Cellulose Nanofibrils with Silica Nanoparticles. *ACS Appl. Mater. Interfaces* **2017**, *9* (44), 39069–39077. https://doi.org/10.1021/acsami.7b13466.

(39) Hachisu, M.; Ohkawa, K.; Yamamoto, H. Preparation of Silk-like Fibers Designed by Self-Assembled Ionic Polypeptides. *Macromol. Biosci.* **2003**, *3* (2), 92–99. https://doi.org/10.1002/mabi.200390015.

(40) Torres-Rendon, J. G.; Schacher, F. H.; Ifuku, S.; Walther, A. Mechanical Performance of Macrofibers of Cellulose and Chitin Nanofibrils Aligned by Wet-Stretching: A Critical Comparison. *Biomacromolecules* **2014**, *15* (7), 2709–2717. https://doi.org/10.1021/bm500566m.

(41) Yudin, V. E.; Dobrovolskaya, I. P.; Neelov, I. M.; Dresvyanina, E. N.; Popryadukhin, P. V.; Ivan'Kova, E. M.; Elokhovskii, V. Y.; Kasatkin, I. A.; Okrugin, B. M.; Morganti, P. Wet Spinning of Fibers Made of Chitosan and Chitin Nanofibrils. *Carbohydr. Polym.* **2014**, *108* (1), 176–182. https://doi.org/10.1016/j.carbpol.2014.02.090.

(42) Wan, A. C. A.; Yim, E. K. F.; Liao, I.-C.; Le Visage, C.; Leong, K. W. Encapsulation of Biologics in Self-Assembled Fibers as Biostructural Units for Tissue Engineering. *J. Biomed. Mater. Res.* **2004**, *71A* (4), 586–595. https://doi.org/10.1002/jbm.a.30158.

(43) Liu, L.; Bai, L.; Tripathi, A.; Yu, J.; Wang, Z.; Borghei, M.; Fan, Y.; Rojas, O. J. High Axial Ratio Nanochitins for Ultrastrong and Shape-Recoverable Hydrogels and Cryogels via Ice Templating. *ACS Nano* **2019**, *13* (3), 2927–2935. https://doi.org/10.1021/acsnano.8b07235.

(44) Wang, L.; Ago, M.; Borghei, M.; Ishaq, A.; Papageorgiou, A. C.; Lundahl, M.; Rojas, O. J. Conductive Carbon Microfibers Derived from Wet-Spun Lignin/Nanocellulose Hydrogels. *ACS Sustain. Chem. Eng.* **2019**, *7* (6), 6013–6022. https://doi.org/10.1021/acssuschemeng.8b06081.

For Table of Contents Use Only

Composite microfibers based on colloidal dispersions of nanochitin of different aspect ratio andalginate are produced by interfacial complexation using a fully sustainable dry spinning process.

Rafael Grande[1,2], Long Bai[2], Ling Wang[2], Wenchao Xiang[2], Olli Ikkala[2,3], Antonio J. F. Carvalho[1], Orlando J. Rojas[2,3,4,]*